

Microfacet Model Regularization for Robust Light Transport Supplemental: Formulas

Johannes Jendersie  and Thorsten Grosch
TU Clausthal, Germany

Abstract

This document summarizes the derivation of formulas from the main paper. Also, additional experiments are provided to justify the decisions in the paper.

1. Bounds on the Microfacet Distribution D

Microfacet distributions are also known as *Normal Distribution Functions* (NDF). The projected area of all facets to the geometric normal \mathbf{n} is the unit area. Thus they are normalized to

$$\int_{\Omega} D(\mathbf{h}) \langle \mathbf{h}, \mathbf{n} \rangle d\omega_{\mathbf{h}} = 1.$$

Variations in this normal distributions are the main reason for variance in the microfacet BSDF models. In the following the upper bounds for the the three most common NDFs are derived, which turns out to be very simple.

1.1. GGX

The GGX distribution [TR75, WMLT07] is defined as

$$D(\mathbf{h}) = \frac{1}{\pi\alpha^2 \left(\langle \mathbf{h}, \mathbf{n} \rangle^2 + \frac{1 - \langle \mathbf{h}, \mathbf{n} \rangle^2}{\alpha^2} \right)^2} \quad (1)$$

and has its maximum at $\mathbf{h} = \mathbf{n}$. Since $\alpha < 1$ the right of the two terms in the denominator grows faster than the left one. This leads to a smaller value of the entire function. The term is zero for $\mathbf{h} = \mathbf{n}$ and thus the maximum is found there. Inserting one for the dot products gives $1/\pi\alpha^2$ as the maximum value.

1.2. Beckmann-Spizzichino

The Beckmann-Spizzichino distribution [BS63] is defined as

$$D(\mathbf{h}) = \frac{1}{\pi\alpha^2 \langle \mathbf{h}, \mathbf{n} \rangle^4} e^{\frac{\langle \mathbf{h}, \mathbf{n} \rangle^2 - 1}{\alpha^2 \langle \mathbf{h}, \mathbf{n} \rangle^2}}. \quad (2)$$

It is usually written with $-\tan^2(\theta_{\mathbf{h}})/\alpha^2$ in the exponent which is equivalent to the above formulation applying some trigonometric identities.

Using derivation we can find its extrema at

$$\langle \mathbf{h}, \mathbf{n} \rangle = \left\{ 1, -\frac{1}{\sqrt{2\alpha}}, \frac{1}{\sqrt{2\alpha}} \right\},$$

where the second one can be ignored, because it only happens for invalid pairs of \mathbf{h} and \mathbf{n} where the two vectors are on different sides of the surface.

The first extremum is a maximum for $\alpha \leq 1/\sqrt{2}$ and a local minimum otherwise. I.e. for $\alpha \leq 1/\sqrt{2}$ we have the same maximum at $\mathbf{h} = \mathbf{n}$ as before.

The third extremum becomes the global maximum for $\alpha > 1/\sqrt{2}$ as is also visible in Figure 1 (left). Inserting $\langle \mathbf{h}, \mathbf{n} \rangle = 1/\sqrt{2\alpha}$ into Equation (2) gives us its value of

$$4\alpha^2 e^{\alpha^2 - 2} / \pi \quad (3)$$

which cannot be solved for α in a closed form. To find an upper bound we first analyze the behavior for $\lim_{\alpha \rightarrow \infty}$. This results in e^{-2} for the exponential term which means that the function's grow is governed by the quadratic term α^2 . To find a function which is always greater than Equation (3) we need to add the value of Equation (3) at $\alpha = 1/\sqrt{2}$ (being $2(e^2 - 1)/\pi e^2$) as offset leading to

$$\hat{D} = \frac{4\alpha^2 + 2(e^2 - 1)}{\pi e^2} \quad (4)$$

as an invertible bound for $\alpha > 1/\sqrt{2}$. It is also possible to use $4\alpha^2/\pi e^2$ directly without the offset term. While not being a strict bound then, it better fits Equation 3 for larger values.

In practice α is often restricted to $[0, 1]$ anyway. In that case regularization for $\alpha \in [1/\sqrt{2}, 1]$ does not make sense ($\alpha = 1$ leads to the global minimum of D over all α) and one can use the very same bound $1/\pi\alpha^2$ as for all previous models, without paying attention to the shifting maximum. However, for unrestricted $\alpha > 1$, which is

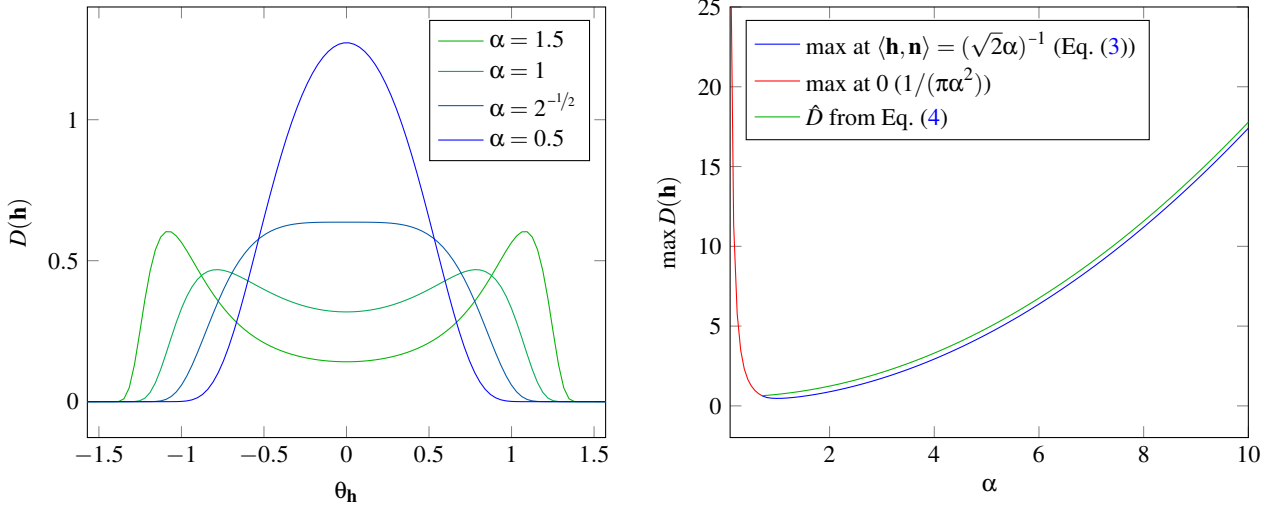


Figure 1: The Beckmann-Spizzichino distribution with varying roughness parameters (left). On the right the value of its maximum is shown with respect to α .

just fine for this model, regularization based on Equation (4) becomes applicable again.

1.3. Blinn-Phong

Usually the Blinn-Phong NDF is parametrized with an exponent n . By setting its normalization term $(n+2)/2\pi$ equal to the normalization term of the other distributions $1/\pi\alpha^2$ we can express n dependent on α and get

$$D(\mathbf{h}) = \frac{n+2}{2\pi} \langle \mathbf{h}, \mathbf{n} \rangle^n = \frac{1}{\pi\alpha^2} \langle \mathbf{h}, \mathbf{n} \rangle^{(2/\alpha^2-2)} \quad (5)$$

It is trivial to see that the maximum is at $\mathbf{h} = \mathbf{n}$ because in all other cases the dot product will become smaller. At this maximum the dot product is one and therefore the entire right side becomes one leaving only $1/\pi\alpha^2$.

2. Bounds on the Microfacet Shadowing G

The next important part of a microfacet model is its self-shadowing term G , which we want to bound together with the denominator $|\langle \vec{\mathbf{w}}, \mathbf{n} \rangle \langle \vec{\mathbf{w}}, \mathbf{n} \rangle|$.

In the V-cavity model [TS67] the shadowing is independent of the roughness parameter and does not necessarily compensate for the cosine denominator at grazing angles. Thus, if using the V-cavity model, our best option is to replace $G/|\langle \vec{\mathbf{w}}, \mathbf{n} \rangle \langle \vec{\mathbf{w}}, \mathbf{n} \rangle|$ with the constant one. The resulting bound is not a strict upper bound which would be infinity in this case.

Using the Smith model [Smi67], where the shadowing is composed of two distribution-dependent functions $G = G_i G_o$, the terms $G_i/|\langle \vec{\mathbf{w}}, \mathbf{n} \rangle|$ and $G_o/|\langle \vec{\mathbf{w}}, \mathbf{n} \rangle|$ are finite in the limit $|\langle \mathbf{w}, \mathbf{n} \rangle| \rightarrow 0$. For the GGX distribution [WMLT07] the result is $2/\alpha$ and for the Beckmann-Spizzichino distribution [BS63] it is $2\sqrt{\pi}/\alpha$.

The Cosine model does not have a closed form term. As an approximation the same term as for the Beckmann distribution can be used [WMLT07].

3. Walter Transmittance Model Refraction Maximization

In Walter's rough transmittance model [WMLT07]

$$\rho_t(\vec{\mathbf{w}}, \vec{\mathbf{w}}) = \frac{D(\mathbf{h}_t)G(\vec{\mathbf{w}}, \vec{\mathbf{w}})(1 - F(\langle \vec{\mathbf{w}}, \mathbf{h}_t \rangle))}{(\eta_i \langle \vec{\mathbf{w}}, \mathbf{h}_t \rangle + \eta_r \langle \vec{\mathbf{w}}, \mathbf{h}_t \rangle)^2} \frac{\eta_t^2 |\langle \vec{\mathbf{w}}, \mathbf{h}_t \rangle \langle \vec{\mathbf{w}}, \mathbf{h}_t \rangle|}{|\langle \vec{\mathbf{w}}, \mathbf{n} \rangle \langle \vec{\mathbf{w}}, \mathbf{n} \rangle|}$$

almost everything can be estimated as in the Torrance-Sparrow reflection model. Solely the term

$$\frac{\eta_t^2}{(\eta_i \langle \vec{\mathbf{w}}, \mathbf{h}_t \rangle + \eta_r \langle \vec{\mathbf{w}}, \mathbf{h}_t \rangle)^2}$$

requires a special treatment. Since we want to obtain a value independent of the directions, the numerator η_t^2 is bounded by $\max(\eta_i, \eta_r)^2$.

For an upper bound we need to minimize the denominator next. The two direction vectors $\vec{\mathbf{w}}, \vec{\mathbf{w}}$ and their half vector \mathbf{h}_t are connected by Snell's law

$$\langle \vec{\mathbf{w}}, \mathbf{h}_t \rangle = -\text{sign}(\langle \vec{\mathbf{w}}, \mathbf{h}_t \rangle) \sqrt{1 - \frac{\eta_t^2}{\eta_i^2} (1 - \langle \vec{\mathbf{w}}, \mathbf{h}_t \rangle^2)} \quad (6)$$

which allows us to express the denominator depending on a single cosine (here $\langle \vec{\mathbf{w}}, \mathbf{h}_t \rangle$). Plugging Equation (6) into the denominator turns out to have its minima at $\langle \vec{\mathbf{w}}, \mathbf{h}_t \rangle = \{-1, 1\}$. Both have a value of $(\eta_i - \eta_r)^2$ with different signs inside the square (which can be ignored). Therefore, the above term is maximized by

$$\frac{\max(\eta_i, \eta_r)^2}{(\eta_i - \eta_r)^2} \quad (7)$$

4. Estimation of the Regularization PDF

In Equation (13) of the paper we introduced $\hat{p} = (\hat{\rho}/\rho) \cdot p$ to simplify the implementation of the necessary MIS weight computation. Here, we show that computing the PDF with respect to $\hat{\alpha}$ yields the same result as computing the ratio when using the V-cavity shadowing model.

Computing the ratios for the microfacet models (given in Equations (4) and (5) in the paper) we get:

$$\frac{\hat{\rho}_r}{\rho_r} = \frac{\hat{\rho}_t}{\rho_t} = \frac{D_{\hat{\alpha}}(\mathbf{h})G_{\hat{\alpha}}(\vec{\mathbf{w}}, \vec{\mathbf{w}})}{D_{\alpha}(\mathbf{h})G_{\alpha}(\vec{\mathbf{w}}, \vec{\mathbf{w}})} \quad (8)$$

where all terms which do not depend on α are canceled trivially.

Using the visible microfacet sampling of Heitz and d'Eon [Hd14] the sampling probabilities for the two models are

$$p_r(\vec{\mathbf{w}}|\alpha) = \frac{D_{\alpha}(\mathbf{h})G_{\alpha}(\vec{\mathbf{w}})F(\vec{\mathbf{w}}, \mathbf{h})}{4|\langle \vec{\mathbf{w}}, \mathbf{n} \rangle \langle \vec{\mathbf{w}}, \mathbf{n} \rangle|} = D_{\alpha}(\mathbf{h})G_{\alpha}(\vec{\mathbf{w}})B_r \quad (9)$$

$$\text{and } p_t(\vec{\mathbf{w}}|\alpha) = \frac{\eta_t^2 D_{\alpha}(\mathbf{h})G_{\alpha}(\vec{\mathbf{w}})(1 - F(\vec{\mathbf{w}}, \mathbf{h}))}{(\eta_t \langle \vec{\mathbf{w}}, \mathbf{h}_t \rangle + \eta_r \langle \vec{\mathbf{w}}, \mathbf{h}_r \rangle)^2 |\langle \vec{\mathbf{w}}, \mathbf{n} \rangle \langle \vec{\mathbf{w}}, \mathbf{n} \rangle|} = D_{\alpha}(\mathbf{h})G_{\alpha}(\vec{\mathbf{w}})B_t \quad (10)$$

For brevity we can summarize all parametrization-independent terms (Fresnel and denominators) as B_r and B_t , respectively. Then we can write for both PDFs:

$$\begin{aligned} \frac{\hat{p}}{\rho} \cdot p(\vec{\mathbf{w}}|\alpha) &= \frac{D_{\hat{\alpha}}(\mathbf{h}) \cdot G_{\hat{\alpha}}(\vec{\mathbf{w}}, \vec{\mathbf{w}})}{D_{\alpha}(\mathbf{h}) \cdot G_{\alpha}(\vec{\mathbf{w}}, \vec{\mathbf{w}})} \cdot D_{\alpha}(\mathbf{h}) \cdot G_{\alpha}(\vec{\mathbf{w}}) \cdot B \\ &= \frac{G_{\hat{\alpha}}(\vec{\mathbf{w}}, \vec{\mathbf{w}})}{G_{\alpha}(\vec{\mathbf{w}}, \vec{\mathbf{w}})} \cdot D_{\hat{\alpha}}(\mathbf{h}) \cdot G_{\alpha}(\vec{\mathbf{w}}) \cdot B \end{aligned} \quad (11)$$

For the V-cavity model [TS67], the shadowing is

$$G(\vec{\mathbf{w}}, \vec{\mathbf{w}}) = \min(1, G(\vec{\mathbf{w}}), G(\vec{\mathbf{w}}))$$

with $G(\vec{\mathbf{w}}) = 2\langle \mathbf{n}, \mathbf{h} \rangle \langle \mathbf{n}, \mathbf{w} \rangle / \langle \mathbf{w}, \mathbf{h} \rangle$.

Thus it is independent of α which allows us to cancel the first factor:

$$(11), \text{ V-cavity} \Rightarrow D_{\hat{\alpha}}(\mathbf{h})G(\vec{\mathbf{w}})B = p(\vec{\mathbf{w}}|\hat{\alpha}).$$

Hence, it is possible to evaluate p with respect to the regularized parameter $\hat{\alpha}$ instead of computing the fraction of BSDFs explicitly.

For the Smith model [Smi67] $G_{\alpha}(\vec{\mathbf{w}}, \vec{\mathbf{w}}) = G_{\alpha}(\vec{\mathbf{w}})G_{\alpha}(\vec{\mathbf{w}})$ depends on α and the distribution model D and cannot be removed that easily. However, we can still simplify the term to reduce the

evaluation cost of a practical implementation:

$$\begin{aligned} (11), \text{ Smith} &\Rightarrow \frac{G_{\hat{\alpha}}(\vec{\mathbf{w}}, \vec{\mathbf{w}})}{G_{\alpha}(\vec{\mathbf{w}}, \vec{\mathbf{w}})} \cdot D_{\hat{\alpha}}(\mathbf{h}) \cdot G_{\alpha}(\vec{\mathbf{w}}) \cdot B \\ &= \frac{G_{\hat{\alpha}}(\vec{\mathbf{w}}) \cdot G_{\hat{\alpha}}(\vec{\mathbf{w}})}{G_{\alpha}(\vec{\mathbf{w}}) \cdot G_{\alpha}(\vec{\mathbf{w}})} \cdot D_{\hat{\alpha}}(\mathbf{h}) \cdot G_{\alpha}(\vec{\mathbf{w}}) \cdot B \\ &= \frac{G_{\hat{\alpha}}(\vec{\mathbf{w}})}{G_{\alpha}(\vec{\mathbf{w}})} \cdot D_{\hat{\alpha}}(\mathbf{h}) \cdot G_{\alpha}(\vec{\mathbf{w}}) \cdot B \\ &= \frac{G_{\hat{\alpha}}(\vec{\mathbf{w}})}{G_{\alpha}(\vec{\mathbf{w}})} \cdot p(\vec{\mathbf{w}}|\hat{\alpha}). \end{aligned}$$

5. Relation of Parameters

In Section 3.4 of the paper we invert the relation between a radius r_0 and our parameter τ_0 . The math behind uses only equivalent transformations as shown below:

$$\begin{aligned} \tau_0 &= \frac{1}{2\pi(1 - \cos(\arctan(r_0/d)))} \\ \Leftrightarrow \frac{1}{2\pi\tau_0} &= 1 - \cos(\arctan(r_0/d)) \\ \Leftrightarrow 1 - \frac{1}{2\pi\tau_0} &= \cos(\arctan(r_0/d)) \\ \Leftrightarrow \frac{2\pi\tau_0 - 1}{2\pi\tau_0} &= \cos(\arctan(r_0/d)) \\ \Leftrightarrow \tan\left(\arccos\left(\frac{2\pi\tau_0 - 1}{2\pi\tau_0}\right)\right) &= \frac{r_0}{d} \\ \Leftrightarrow d \tan\left(\arccos\left(\frac{2\pi\tau_0 - 1}{2\pi\tau_0}\right)\right) &= r_0 \end{aligned}$$

By using $\tan(\arccos(x)) = \sqrt{1-x^2}/x$ we can get rid of the trigonometric functions, too:

$$\begin{aligned} \Leftrightarrow r_0 &= d \sqrt{1 - \left(\frac{2\pi\tau_0 - 1}{2\pi\tau_0}\right)^2} \frac{2\pi\tau_0}{2\pi\tau_0 - 1} \\ \Leftrightarrow r_0 &= d \sqrt{\frac{4\pi^2\tau_0^2 - (2\pi\tau_0 - 1)^2}{4\pi^2\tau_0^2}} \frac{2\pi\tau_0}{2\pi\tau_0 - 1} \\ \Leftrightarrow r_0 &= d \sqrt{4\pi^2\tau_0^2 - (2\pi\tau_0 - 1)^2} \frac{1}{2\pi\tau_0 - 1} \\ \Leftrightarrow r_0 &= d \frac{\sqrt{4\pi\tau_0 - 1}}{2\pi\tau_0 - 1} \end{aligned}$$

Next, we insert the above r_0 in Equation (14) of the paper, yielding the iteration dependent parameter

$$r_N = r_0 \cdot N^{-1/6} = d \frac{\sqrt{4\pi\tau_0 - 1}}{2\pi\tau_0 - 1} \cdot N^{-1/6}. \quad (12)$$

In the last step we reinsert r_N in Equation (15) of the paper:

$$\tau_N = \frac{1}{2\pi \left[1 - \cos\left(\arctan\left(d \frac{\sqrt{4\pi\tau_0 - 1}}{2\pi\tau_0 - 1} \cdot N^{-1/6} / d\right)\right)\right]} \quad (13)$$

where d gets canceled out.

6. MIS for Virtual Merges

The virtual merge strategy samples the BSDF and accepts the connection if the sample is within the allowed cone of the connection direction. To compute the probability of a successful connection we need to compute

$$p_{\text{acc}} = \int_{\Omega} p(\vec{\omega}, \vec{\omega}) d\vec{\omega}$$

where Ω is the cone whose solid angle is $|\Omega|$. As done in VCM [GKDS12, HPJ12] this integral can be approximated with a single sample $|\Omega|p(\vec{\omega}, \vec{\omega})$. The solid angle can also be expressed by our parameter with $|\Omega| = 1/\tau$. This is because a uniform PDF over the cone is $1/|\Omega|$ and τ defines the maximum value of this PDF. We get the approximation

$$p_{\text{acc}} \approx \frac{p(\vec{\omega}, \vec{\omega})}{\tau}. \quad (14)$$

Now, we insert p_{acc} into our path probability. This would require several changes to the MIS computation function. However, it is possible to change the stored PDF values at the vertices to have a modification that is simpler to implement. Since we always need ratios between path probabilities and not the probabilities themselves, we can divide the PDFs of all other paths instead of multiplying with the current one. Hence, if a vertex stored $p(\vec{\omega}, \vec{\omega})$ before, it is possible to store $p(\vec{\omega}, \vec{\omega})/p_{\text{acc}}$ instead, because the stored PDF is used for the path PDF of all but the current path. By inserting Equation (14) this simplifies to τ .

This means that a connection with a random acceptance is equal to a continuation of the random walk. The difference is that the random walk is always accepted while the virtual merge depends on the solid angle or its alias $1/\tau$ – which is all what remains. Note that this argumentation is based on the single sample approximation and not a fundamental law. The implicit assumption of the approximation is that the sample is within the cone with a probability proportional to the size of the cone.

7. Convergence

Finally, we want to present a convergence series which shows the reduction of both noise and bias. In the context of regularization it is difficult to define a ground truth, as the bias is part of the desired outcome. Pure *specular* paths with a point light source and a pin-hole camera have no contribution in truth. However, they are also physically implausible. Hence, blurring those light paths virtually increases plausibility of the result.

Therefore, our reference images are rendered with the same configuration (regularized VCM), but for 10000 iterations. The other closeups show the 1024th iteration of the four tested configurations. Due to progressive radius shrinking, the parameter τ becomes roughly twice as large between 1024 and 10000 iterations.

The graph showing the noise (σ/N) clearly shows a monotonous decrease of the variance in all four methods. The regularized versions have more noise due to the *shiny* effects. However, regularization increases the similarity to the desired reference as visible in the right plot. Especially, the BPT profits from the regularization.

References

- [BS63] BECKMANN P., SPIZZICHINO A.: *The Scattering of Electromagnetic Waves from Rough Surfaces*. International Series of Monographs on Electromagnetic Waves. vol. 4. Pergamon Press, 1963. 1, 2
- [GKDS12] GEORGIEV I., KRIVÁNEK J., DAVIDOVIČ T., SLUSALLEK P.: Light Transport Simulation with Vertex Connection and Merging. *ACM Transactions on Graphics (Proc. of SIGGRAPH Asia)* 31, 6 (2012), 192:1–192:10. doi:10.1145/2366145.2366211. 4
- [Hd14] HEITZ E., D'EON E.: Importance Sampling Microfacet-Based BSDFs Using the Distribution of Visible Normals. *Computer Graphics Forum (CGF)* 33, 4 (2014), 103–112. doi:10.1111/cgf.12417. 3
- [HPJ12] HACHISUKA T., PANTALEONI J., JENSEN H. W.: A Path Space Extension for Robust Light Transport Simulation. *ACM Transactions on Graphics (Proc. of SIGGRAPH Asia)* 31, 6 (Nov. 2012), 191:1–191:10. doi:10.1145/2366145.2366210. 4
- [Smi67] SMITH B. G.: Geometrical Shadowing of a Random Rough Surface. *IEEE Transactions on Antennas and Propagation* 15, 5 (Sept. 1967), 668–671. doi:10.1109/TAP.1967.1138991. 2, 3
- [TR75] TROWBRIDGE T. S., REITZ K. P.: Average irregularity representation of a rough surface for ray reflection. *Journal of the Optical Society of America* 65, 5 (May 1975), 531–536. doi:10.1364/JOSA.65.000531. 1
- [TS67] TORRANCE K. E., SPARROW E. M.: Theory for Off-Specular Reflection From Roughened Surfaces. *Journal of the Optical Society of America* 57, 9 (Sept. 1967), 1105–1114. doi:10.1364/JOSA.57.001105. 2, 3
- [WMLT07] WALTER B., MARSCHNER S. R., LI H., TORRANCE K. E.: Microfacet Models for Refraction Through Rough Surfaces. In *Proc. of Eurographics Symposium on Rendering (EGSR)* (2007), Eurographics Association, pp. 195–206. doi:10.2312/EGWR/EGSR07/195-206. 1, 2

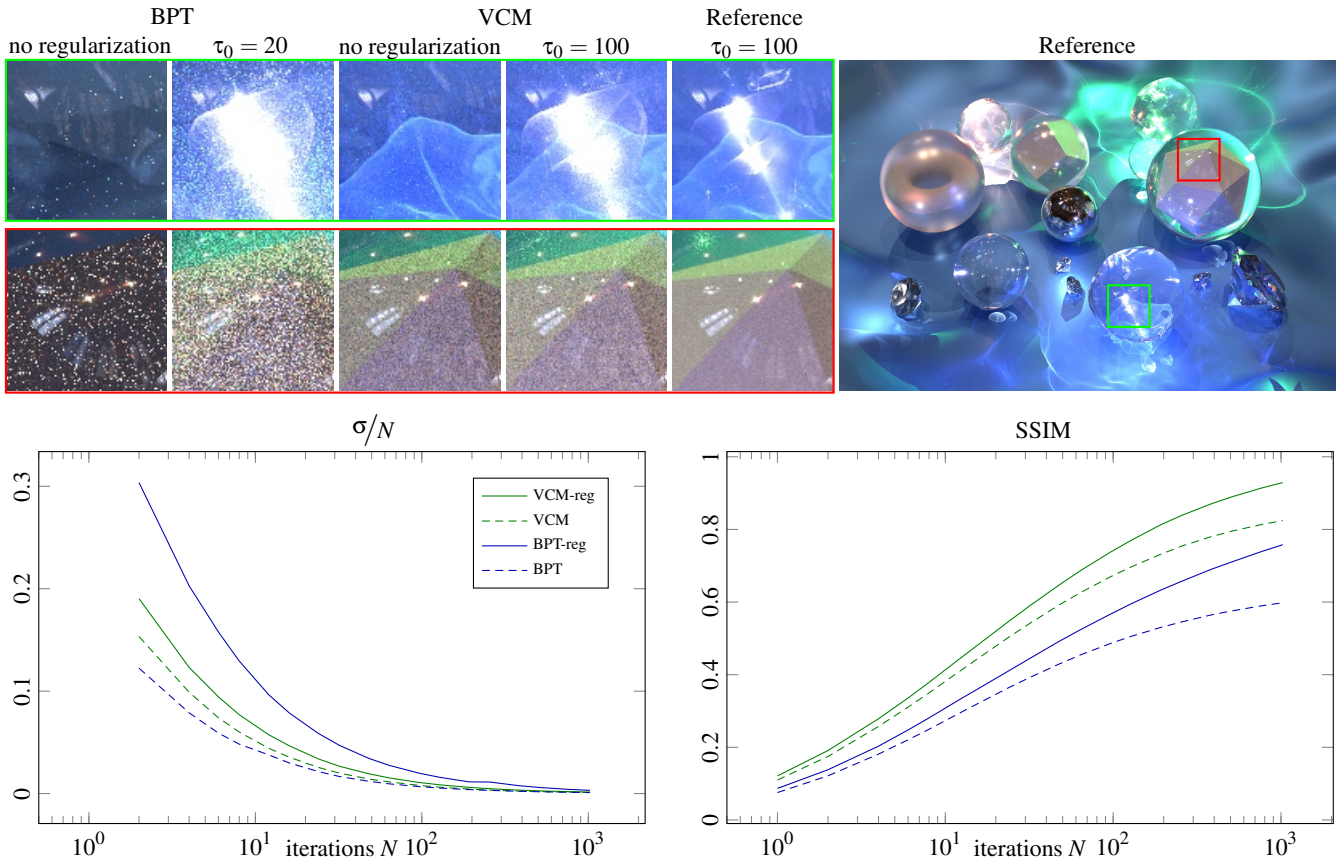


Figure 2: Convergence series demonstrating the reduction of bias and noise if using progressive, selective regularization. The upper row of the closeups clearly shows a reduction of the blurred shiny effect (i.e. a bias reduction). The lower row demonstrates the noise differences.